# Finite-Element Modeling and Calibration of Temperature Prediction of Hydrating Portland Cement Concrete Pavements

Jin-Hoon Jeong[1] and Dan G. Zollinger, P.E.[2]

**Abstract:** The temperature profiles in a hydrating concrete slab are produced by a two-dimensional finite-element method software tool, TMAC[2] (temperature and moisture analysis for curing concrete), as a function of time and ambient boundary conditions described in this paper. To include the effect of the heat of vaporization, heat flux due to evaporation is included in the boundary condition of heat transfer at the slab surface in addition to the effects of surface humidity, effective curing thickness, and surface moisture emissivity on the rate of evaporation. Thermal conductivity is back-calculated using the data collected from laboratory measurements toward the improvement of the modeling of thermal conductivity. Theoretically, the material properties determined in this manner should facilitate accurate temperature prediction. Thus, temperature prediction in hardening concrete pavements under various conditions can be effectively calibrated by improved material characterization. To this end, this paper provides the basis of a calibration protocol.

**DOI:** 10.1061/(ASCE)0899-1561(2006)18:3(317)

**CE Database subject headings:** Concrete pavements; Temperature; Heat transfer; Finite element method; Evaporation; Thermal factors.



## Introduction

The temperature and moisture history and distribution of hardening concrete is of great interest during pavement construction for purposes such as crack control and saw-cut timing, assessment of curing effectiveness, estimation of drying shrinkage and thermal expansion, and evaluation of concrete strength development. In construction, these items are often impacted by ambient weather conditions because of their effect on the rate of strength gain or hydration of the concrete mixture. Consequently, it would be advantageous to have analytical models that could be used to estimate the hardening state of concrete at any time during the curing cycle in terms of the environmental conditions and the method of curing. Accordingly, a computer-based model, temperature and moisture analysis for curing concrete (TMAC[2]), has been developed recently at the Texas Transportation Institute.

A key aspect of the TMAC[2] program is its consideration of heat loss and gain due to evaporation and condensation of moisture at the slab surface. Another significant advantage of the model is its consideration of the interaction between the temperature and moisture effects in the material property models and boundary conditions to enhance accuracy of the analysis results. These are important capabilities in making accurate predictions of the spatial and diurnal distribution of temperature in hardening concrete pavement.

The user-friendly input parameters of TMAC[2] are categorized into four groups. One group consists of strength and heat development material properties derived from laboratory testing; another consists of environmental conditions such as ambient temperature, ambient humidity, wind speed, and solar radiation; construction conditions such as the method of curing make up the third group; and the fourth relates to such geometric inputs as slab thickness.

Temperature distributions in concrete pavement are estimated by analyzing the transient heat transfer between the concrete and the surrounding conditions, as represented by the boundary value equations where the effects of environmental factors such as air temperature, wind velocity, solar radiation, and heat of vaporization are accounted for. The heat of hydration should be considered to enhance the accurate estimation of temperature distributions of early-age concrete in a pavement structure. The hydration process generates internal heat, which influences the rate of chemical reactions of the cementitious materials and water while the environmental conditions influence concrete temperature and moisture conditions at the surface.

Characterization of thermal conductivity is important in order to accurately model heat movements in a concrete pavement. Using temperature data collected from a test slab, the back-calculation of thermal conductivity is subsequently described by a transformation of the governing equation of heat transfer. The back-calculated results formed the basis of a material model to calibrate the predicted temperature distribution under various curing conditions and mix proportions.

[1]Assistant Professor, School of Civil and Environmental Engineering, Inha Univ., 253 Yonghyeon-dong, Nam-gu, Incheon 402-751, Korea. E-mail: ihj@inha.ac.kr

[2]Associate Professor, Dept. of Civil Engineering, Texas A&M Univ., 503E, CE/TTI Building, College Station, TX 77843-3136. E-mail: d-zollinger@tamu.edu

Note. Associate Editor: Christopher K. Y. Leung. Discussion open until November 1, 2006. Separate discussions must be submitted for individual papers. To extend the closing date by one month, a written request must be filed with the ASCE Managing Editor. The manuscript for this paper was submitted for review and possible publication on February 19, 2004; approved on February 8, 2005. This paper is part of the ***Journal of Materials in Civil Engineering***, Vol. 18, No. 3, June 1, 2006. ©ASCE, ISSN 0899-1561/2006/3-317–324/$25.00.



J. Mater. Civ. Eng. 2006.18:317-324.

## Governing Equation of Heat Transfer

The governing equation of heat transfer for temperature prediction in an early-age concrete pavement taking heat of hydration and ambient temperature conditions into account is (Klemens 1969; Incropera and DeWitt 1996)

$$\frac{\partial}{\partial x}\left(k_x\frac{\partial T}{\partial x}\right)+\frac{\partial}{\partial y}\left(k_y\frac{\partial T}{\partial y}\right)+Q_h=\rho c_p\frac{\partial T}{\partial t} \tag{1}$$

where $T$=concrete temperature (°C); $t$=time (h); $x$, $y$=coordinates in concrete pavement (m); $k_x$, $k_y$=thermal conductivities of concrete (W/m/°C); $Q_h$=heat of hydration (W/m$^3$); $\rho$=concrete density (kg/m$^3$); and $c_p$=specific heat of concrete (J/kg/°C);.

The density ($\rho$) and specific heat ($c_p$) of concrete in Eq. (1) are basic material properties determined by laboratory and ASTM test procedures that are not elaborated here. The heat of hydration of concrete ($Q_h$) in Eq. (1) is the amount of heat released into the surroundings of the concrete pavement due to the hydration process. The heat of hydration is mathematically defined as (Emborg 1989)

$$Q_h=H_u C\alpha\frac{\lambda_1\kappa_1}{t_1}\frac{[\ln(\tau)]^{-(1+\kappa_1)}}{\tau}\cdot\exp\left[-\frac{E}{R}\left(\frac{1}{T+273}-\frac{1}{T_r+273}\right)\right] \tag{2}$$

where $H_u$=total heat of hydration (J/g); $C$=cement content (g/cm$^2$); $\lambda_1$, $\kappa_1$, $t_1$=hydration shape and time parameters; $\tau$=age parameter=$1+t_e/t_1$; $t_e$=equivalent age; $\alpha$=degree of hydration; $E$=activation energy (J/mol); $R$=universal gas constant (=8.3144 J/mol/°C); and $T_r$=reference temperature (=20°C).

The equivalent age ($t_e$) is predicted by the Arrhenius maturity theory and then used in the calculation of degree of hydration of concrete as (Emborg 1989; Bazant and Najjar 1972)

$$t_e=\sum_{t=0}^{\text{age}}\beta_T\beta_H\Delta t \tag{3a}$$

$$\alpha=\exp[-\lambda_1(\ln\tau)^{-\kappa_1}] \tag{3b}$$

where $\beta_T=\exp\{-E[1/(T+273)-1/(T_r+273)]/R\}$; $\beta_H=1/[1+(5-5H)]$ (Jeong 2003); and $H$=humidity of concrete.

## Boundary Conditions

The environmental effects associated with concrete pavement construction are prevalent at both the pavement surface and the bottom. The initial and boundary conditions are summarized as follows:

$$T=T_0 \quad \text{initial condition} \tag{4a}$$

$$-k\nabla T\cdot n+q''_{\text{conv}}+q''_r-q''_s+q''_e=0$$

$$\text{boundary condition at pavement surface} \tag{4b}$$

$$-k\nabla T\cdot n=0 \quad \text{boundary condition at pavement bottom} \tag{5}$$

where $T_0$=initial temperature (°C); $k$=thermal conductivity (W/m/°C); $q''_{conv}$=heat flux due to convection (W/m$^2$); $q''_r$=heat flux due to irradiation (W/m$^2$); $q''_s$=solar radiation absorption (W/m$^2$); $q''_e$=heat flux due to evaporation (W/m$^2$); $\nabla$=gradient notation; and $n$=unit direction of heat flow by vector notation.

Thus while concrete pavement, convection, radiation, and evaporation play a dominant role in transferring heat between the slab surface and the surrounding air, as indicated by Eq. (4), conduction plays a separate role in transferring heat within the slab, as depicted by Eq. (5). The different types of heat transfer shown in the boundary conditions are consequently described.

### *Conduction*

Heat conduction is explained as heat transfer from points of higher temperature to points of lower temperature. Heat energy is transferred within a slab due to interaction between the particles at different temperatures. Molecules at a high temperature are said to have high energy, which makes the molecules themselves randomly translate and internally rotate and vibrate. Conduction can be expressed by using Fourier's law in the form of a rate equation; for a temperature distribution $T$ in one dimension it can be expressed as a function of direction $x$ as (Klemens 1969; ASHRAE 1972)

$$q''_{\text{cond}}=-k\frac{dT}{dx}$$

where the conductive heat flux, $q''_{cond}$(W/m$^2$), is the heat transfer rate in the $x$-direction per unit area perpendicular to the direction of transfer.

### *Convection*

Heat energy is transferred from a slab surface to the surrounding environment by convection due to currents of air flow due to wind. In addition, this convection is facilitated by random molecular motion in the air flow. If the temperatures between a slab surface and a wind flow differ, temperature in the air flow above the slab will vary from $T_s$ at the slab surface to $T_a$ in the flow far above the slab surface. Convection heat transfer is expressed as (Says and Crawford 1980; Kaviany 1994)

$$q''_{\text{conv}}=h_c(T_s-T_a)$$

where $h_c$(W/m$^2$/°K)=convective heat transfer coefficient. An empirical formula was suggested to relate the convection heat transfer coefficient ($h_c$) to wind velocity and roughness of slab surface (Branco et al. 1992)

$$h_c=6+3.7v$$

where $v$=wind speed (m/s) and 6 W/m$^2$/°K represents an average slab surface roughness without wind effects. The heat transfer coefficient proportionally increases with increase of wind speed.

### *Irradiation*

Irradiation transfers heat energy by electromagnetic waves while conduction and convection require a material medium. Irradiation for a concrete pavement is determined on the basis that a slab surface at temperature $T_s$ radiates to a much larger surface at temperature $T_a$ surrounding the slab surface. Irradiation heat transfer can be expressed as (Siegel and Howell 1981; Meinel and Meinel 1976)

$$q''_r=\varepsilon\sigma(T_s^4-T_a^4)$$

where $\varepsilon$=heat emissivity; $\sigma$=Stefan-Boltzmann constant (=5.67×10$^{-8}$W/m$^2$/°K$^4$); $T_s$=absolute temperature at surface of concrete slab (°K); and $T_a$=absolute temperature of ambient (°K).



J. Mater. Civ. Eng. 2006.18:317-324.

The heat emissivity, which ranges from 0 to 1, is a radiative property of a slab surface and provides a measure of how efficiently the surface emits energy relative to a blackbody.

### Solar Radiation

Solar radiation absorbed directly into a concrete slab surface causes the surface of the slab to be heated more rapidly than the interior region. This effect contributes to a temperature gradient through the depth of the slab (Branco et al. 1992; Hsieh et al. 1989). The solar radiation absorption into a slab surface is influenced by the time of day or year, latitude, cloudiness, and so on (Branco et al. 1992; Chapman 1982; Taljaston 1987). The following equation is used to consider solar radiation absorption:

$$q_s'' = \alpha_s q_{\text{solar}}''$$

where $\alpha_s$=surface heat absorptivity of concrete (=0.5–0.6) (Chapman 1982); and $q_{solar}''$=instantaneous solar radiation ($W/m^2$).

### Heat Flux due to Evaporation

Including heat flux due to evaporation in the boundary condition of heat transfer at the slab surface is important to accurately predict the temperature distribution in a hydrating concrete pavement. A limited number of published temperature prediction models consider the evaporation effects in their boundary conditions (Kapila et al. 1997). There have been many efforts to develop concrete temperature prediction models that can be easily used although they ignore the effect of heat flux due to evaporation in their boundary conditions (Yang 1996; Ruiz et al. 2001). Heat flux due to evaporation can be calculated by

$$q_e'' = EH_v \tag{6}$$

where $E$=rate of evaporation ($kg/m^2/h$ or $W/m^3$); and $H_v$=heat of vaporization of water=$597.3-0.564T_s$ (cal/g) (Linsley et al. 1975) =$427(597.3-0.564T_s)$ (m).

Because none of the existing evaporation models considered the drying characteristics of concrete, a modified version of Penman's evaporation model was prescribed as (Jeong and Zollinger 2003)

$$E = \delta \frac{q_s''}{H_v} + J \tag{7}$$

where $\delta$=calibration factor for moisture condition of concrete surface; and $J$=rate of evaporation from concrete due to convective heat transfer, irradiation, and aerodynamic effects ($kg/m^2/h$).

The rate of evaporation under laboratory curing conditions (i.e., nonsolar effects) shown in Eq. (7) is expressed by a model proposed by Bazant and Najjar (1972) as

$$J = B \ln \frac{H_s}{H_a} \tag{8}$$

where $B$=surface moisture emissivity ($kg/m^2/h$); $H_s$=concrete surface humidity; and $H_a$=ambient humidity.

The surface moisture emissivity was formulized as functions of effective curing thickness ($L$), laboratory-derived coefficients ($a-f$), and wind speed ($v$) during and after bleeding, respectively (Jeong and Zollinger 2003)

$$B = a + b \exp(-L) + cv^2 \quad \text{during bleeding} \tag{9}$$

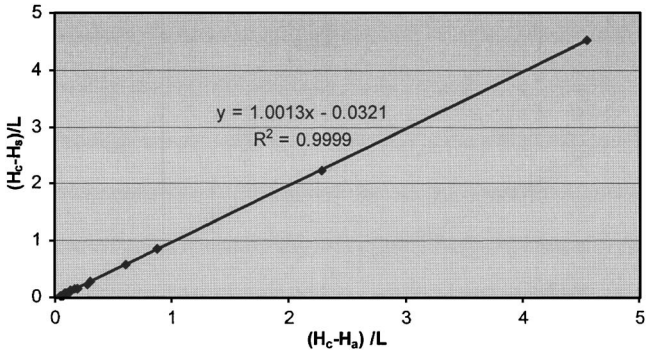


**Fig. 1.** Relationship among ambient humidity, surface humidity, concrete humidity at 1.9 cm (0.75 in.) below top surface, and effective curing thickness

$$B = d + \frac{e \ln L}{L} + fv^{2.5} \quad \text{after bleeding} \tag{10}$$

expressed in units of surface moisture emissivity ($kg/m^2/h$), effective curing thickness (cm), and wind speed (m/s). The effective curing thickness shown in Eqs. (9) and (10) was originally proposed by Bazant and Najjar (1972) and was used by Jeong and Zollinger (2003) to represent the effectiveness of various curing methods

$$L = \frac{\ln \dfrac{H_s}{H_a}}{\dfrac{\partial H_s}{\partial x}} \tag{11}$$

As explained through Eqs. (6)–(11), solar radiation, wind speed, ambient humidity, and concrete humidity at both the surface and 1.9 cm (0.75 in.) below the top surface are required to calculate the heat flux due to evaporation. Among those, solar radiation, wind speed, and ambient humidity can be predicted by a database of a local weather station where the pavement is constructed. Concrete humidity can be predicted by the humidity module of TMAC$^2$, which uses surface humidity as its boundary condition. Surface humidity has been assumed to be equivalent to the ambient humidity to simplify the moisture boundary condition at the top surface (Parrott 1988, 1991). Note, however, that the concrete surface humidity is not the same as the ambient humidity due to such factors as the presence of a curing compound (Jeong and Zollinger 2003). Consequently, surface humidity was represented as a function of ambient humidity ($H_a$), concrete humidity at 1.9 cm (0.75 in.) below the top surface ($H_c$), and effective curing thickness ($L$) (Fig. 1) to account for the effect of a curing compound based on a relationship derived from laboratory curing test results (Jeong and Zollinger 2003)

$$H_s = aH_a + bH_c + cL \tag{12}$$

where $a$ to $c$ are laboratory-derived coefficients.

## Finite-Element Modeling

For the purpose of numerical modeling, a concrete pavement section is discretized into a mesh with 120 elements (5 columns $\times$24 rows) and 539 nodal points. Nine-node rectangular elements are used to represent the pavement section. To obtain a numerical solution of temperature distribution in the concrete pavement sec-



J. Mater. Civ. Eng. 2006.18:317-324.

tion, the governing equation [Eq. (1)] and boundary conditions [Eqs. (4) and (5)] need to be transformed into their equivalent finite-element forms. To construct a variation form for the solution of the partial differential equation, the procedure involves multiplying the governing equation with a weight function $w$ and integrating the product over the element domain $\Omega^{(e)}$

$$0 = \int_{\Omega^{(e)}} w\left[\rho c_p \frac{\partial T}{\partial t} - \frac{\partial}{\partial x}\left(k_x \frac{\partial T}{\partial x}\right) - \frac{\partial}{\partial y}\left(k_y \frac{\partial T}{\partial y}\right) - Q_h\right] dxdy \tag{13}$$

The weight function $(w)$=arbitrary continuous function differentiable once with respect to $x$ and $y$. Then Eq. (13) is integrated by parts to give

$$0 = \int_{\Omega^{(e)}} \left[k_x \frac{\partial w}{\partial x}\frac{\partial T}{\partial x} + k_y \frac{\partial w}{\partial y}\frac{\partial T}{\partial y} + w\rho c_p \frac{\partial T}{\partial t} - wQ_h\right] dxdy - \int_{\Gamma^{(e)}} w\left(k_x \frac{\partial T}{\partial x} n_x + k_y \frac{\partial T}{\partial y} n_y\right) d\Gamma \tag{14}$$

where $n_x$ and $n_y$=rectangular component of $n$, denoting the unit vector normal to the boundary $\Gamma^{(e)}$ of the element domain $\Omega^{(e)}$. Eq. (14) is the variational form of Eq. (1) and forms the basis of the finite-element model.

Suppose that $T$ is approximated using the Ritz method by the expression (Reddy 1984; Timoshenko and Goodier 1970)

$$T(x,y,t) = \sum_{j=1}^{9} T_j(t)\psi_j(x,y) \tag{15}$$

$$w = \psi_i, \quad i = 1,2,\ldots,9 \tag{16}$$

where $T_j$=values of $T$ at the points $(x_j, y_j)$ and $\psi_j$=quadratic interpolation functions. The number of $T_j$ and $\psi_j$ is nine, in accordance with the number of nodes per element. The specific forms of $\psi_j$ are derived for the nine-node rectangular elements of the problem, according to a systematic procedure provided by the finite-element method (Timoshenko and Goodier 1970). Substitution of Eq. (15) for $T$ and Eq. (16) for $w$ into Eq. (14) yields

$$[M^{(e)}]\{\dot{T}\} + [K^{(e)}]\{T\} = \{F^{(e)}\} \tag{17}$$

where

$$M_{ij}^{(e)} = \int_{\Omega^{(e)}} \rho c_p \psi_i \psi_j dxdy$$

$$K_{ij}^{(e)} = \int_{\Omega^{(e)}} \left(k_x \frac{\partial \psi_i}{\partial x}\frac{\partial \psi_j}{\partial x} + k_y \frac{\partial \psi_i}{\partial y}\frac{\partial \psi_j}{\partial y}\right) dxdy + h_c \int_{\Gamma^{(e)}} \psi_i \psi_j d\Gamma$$

$$F_i^{(e)} = \int_{\Gamma^{(e)}} \psi_i \left(k_x \frac{\partial T}{\partial x} n_x + k_y \frac{\partial T}{\partial y} n_y\right) d\Gamma + \int_{\Omega^{(e)}} \psi_i Q_h dxdy$$

$$\{T\} = [T_1(t), T_2(t), \ldots, T_9(t)]^T$$

For an element with a portion of $\Gamma^{(f)}$ coinciding with boundary $\Gamma$ of the whole domain $\Omega$, $F_i^{(f)} = Q_{1i} + Q_{2i} + Q_{3i} + Q_{4i} + Q_{5i}$, where $Q_{1i}$ is related to the heat of hydration, and the remainder of right-hand side terms in the equation is relevant to the boundary conditions such as convection, irradiation, solar radiation, and evaporation.

Each element is connected with one or more elements at its nodes. Since $T$ is continuous, the values of $T$ over the adjacent elements should be the same at the connecting nodes. To express this correspondence mathematically for the sake of assembly of element equations, the values of $T$ at the global nodes are labeled with $U_1, U_2, \ldots, U_N$, where $N$=total number of global nodes. The correspondence between the element nodal values and the global nodal values is established. These relations are called interelement continuity conditions. Correct members from the matrices of correct elements are superimposed according to interelement continuity conditions to give the global or assembled equation of the modeling

$$[M]\{\dot{U}\} + [K]\{U\} = \{F\} \tag{18}$$

where $\{U\} = [U_1, U_2, \ldots, U_N]^T$.

An $\alpha$ family of approximation may be introduced to approximate a weighted average of the time derivatives of the temperature $\{U\}$ at two consecutive time steps by linear interpolation of the values of the temperatures at the two time steps

$$(1-\alpha)\{\dot{U}\}_s + \alpha\{\dot{U}\}_{s+1} = \frac{\{U\}_{s+1} - \{U\}_s}{\Delta t_{s+1}} \tag{19}$$

where $\alpha$ ranges from 0 to 1, $\{\ \}_s$ refers to the values of the enclosed quantity at time $t=t_s$, the symbol dot in $\{\ \}$ denotes the first derivative with respect to time $t$, and $\Delta t$ denotes the time increment, that is, $\Delta t_{s+1} = t_{s+1} - t_s$. A number of different schemes use different $\alpha$:

- $\alpha=0$ as a forward difference method;
- $\alpha=0.5$ as the Crank-Nicolson method; and
- $\alpha=1$ as a backward difference method.

To obtain an unconditionally stable solution, the Crank–Nicolson method is used in the program (Reddy 1993; Bathe 1982). Rearranging Eq. (18) with Eq. (19)

$$[\hat{\mathbf{M}}]\{U\}_{s+1} = [\hat{K}]\{U\}_s + \{\mathbf{F}\}_{s,s+1} \tag{20}$$

where

$$[\hat{\mathbf{M}}] = [\mathbf{M}] + \alpha\Delta t_{s+1}[K]$$

$$[\hat{K}] = [\mathbf{M}] - (1-\alpha)\Delta t_{s+1}[K]$$

$$\{\mathbf{F}\}_{s,s+1} = \Delta t_{s+1}[\alpha\{\mathbf{F}\}_{s+1} + (1-\alpha)\{\mathbf{F}\}_s]$$

Since the column vector $\{F\}$ is known at all times, $\{F\}_{s+1}$ is known in advance. The solution $\{U\}_{s+1}$ at time $t=t_{s+1}$ is obtained in terms of the solution $\{U\}_s$ at time $t_s$ by inverting the matrix $[M]$. At time $t=0$, the solution is known from the initial conditions of the problem, and therefore Eq. (20) can be used to obtained the solution at $t=\Delta t_1$, and so forth.

## Validation of Thermal FEM Analysis

A 30.5 cm (12 in.) thick test slab was constructed at the Riverside Campus Annex test facility of Texas A&M University, located in Bryan, Tex. (Jeong and Zollinger 2005). To calculate the heat of hydration of the test slab, parameters of Eq. (2) such as total heat of hydration, activation energy, hydration shape, and time parameters were found from laboratory tests. A superinsulated steel Qdrum semiadiabatic calorimeter manufactured by Digital Site Systems, Inc. was used to calculate total heat of hydration of the test slab. The calorimeter measures the heat energy accumulated in the concrete due to heat of hydration and the heat flow through the superinsulated wall of the calorimeter. Concrete was placed in



J. Mater. Civ. Eng. 2006.18:317-324.

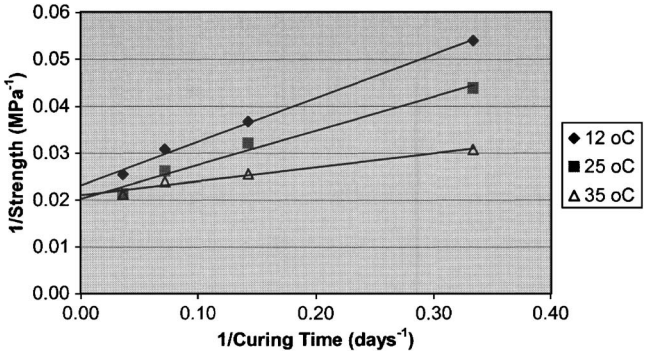


**Fig. 2.** Reciprocal of mortar cube strength versus reciprocal of age

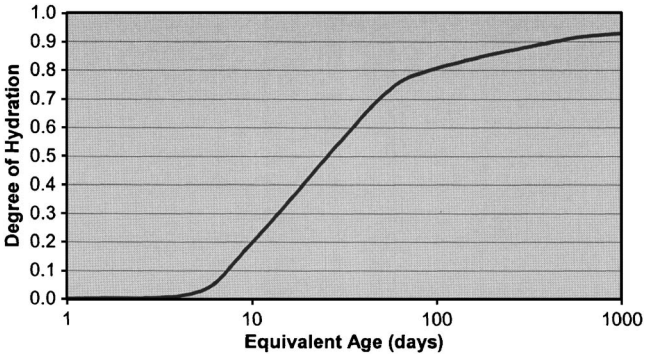


**Fig. 4.** Degree of hydration of test slab with equivalent age

a $15.2 \times 30.5$ cm ($6 \times 12$ in.) plastic cylinder mold. This specimen was put inside the calorimeter with a tightly sealed and insulated lid. Data collected from a datalogger connected to the calorimeter indicated 385 J/g of total heat of hydration from the concrete specimen.

The activation energy was determined in accordance with ASTM (1999) using mortar cube specimens. Mortar was placed in brass cubic molds with 5.1 cm (2 in.) sides, and the specimens were submerged temperature-controlled water baths at 12, 25, and 35 °C, respectively. The specimens were demolded immediately before a compressive strength test performed at 3, 7, 14, and 28 days using a universal hydraulic testing machine. Ultimate compressive strengths for each curing temperature were estimated by interceptions of best-fit straight lines of a reciprocal of average cube strength versus a reciprocal of age, as shown in Fig. 2. The activation energy of 31.4 kJ/mol was determined by the slope of the best-fit straight line of the natural logarithm of the reciprocal of age versus the reciprocal of absolute curing temperature, as shown in Fig. 3. The slope of the line is the value of activation energy divided by the gas constant (8.3144 J/mol/°K).

To get the shape and time parameters $\lambda_1$, $\kappa_1$, and $t_1$ shown in Eqs. (2) and (3), compressive strength tests of the $10.2 \times 20.3$ cm ($4 \times 8$ in.) standard cylinder specimens were made at 1, 3, 7, and 14 days after placement. The parameters were determined by the relative strengths (degree of hydration) and maturity of the specimens using least-squares linear regression analysis. The values of the parameters for the mix proportion used in the test slab were found to be 0.69, 1.52, and 13, respectively. The curve of degree of hydration ($\alpha$) with equivalent age ($t_e$) obtained by Eq. (3) is shown in Fig. 4.

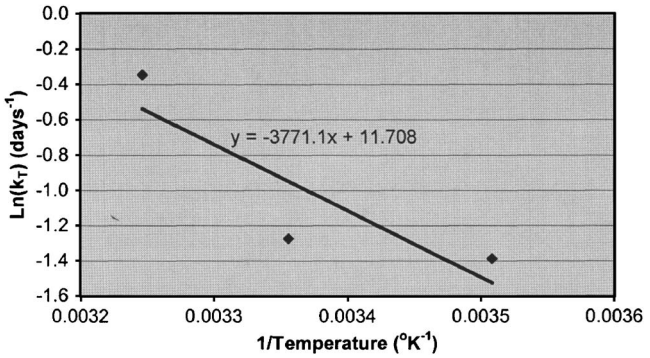


**Fig. 3.** Logarithm of rate constant of mortar cube versus reciprocal of curing temperature

### *Back-Calculation and Model Calibration*

Thermal conductivity is a parameter that dominates the heat movements in concrete pavement. For better prediction of temperature in hardening concrete, the thermal conductivity back-calculated from the governing equation of heat transfer [Eq. (1)] as

$$k = \frac{\rho c_p \dfrac{\partial T}{\partial t} - Q_h}{\dfrac{\partial^2 T}{\partial x^2}} \tag{21}$$

The back-calculated values are expected to yield valid estimates of thermal conductivity over time and to more accurately predict temperature in hardening concrete. The temperature and moisture profiles of a concrete cylinder with a 20.3 (8 in.) diameter and 30.5 cm (12 in.) height were characterized in the laboratory by using third-degree polynomial fits based on the data measured at 2.5, 7.6, and 12.7 (1, 3, and 5 in.) (Fig. 5). Temperature

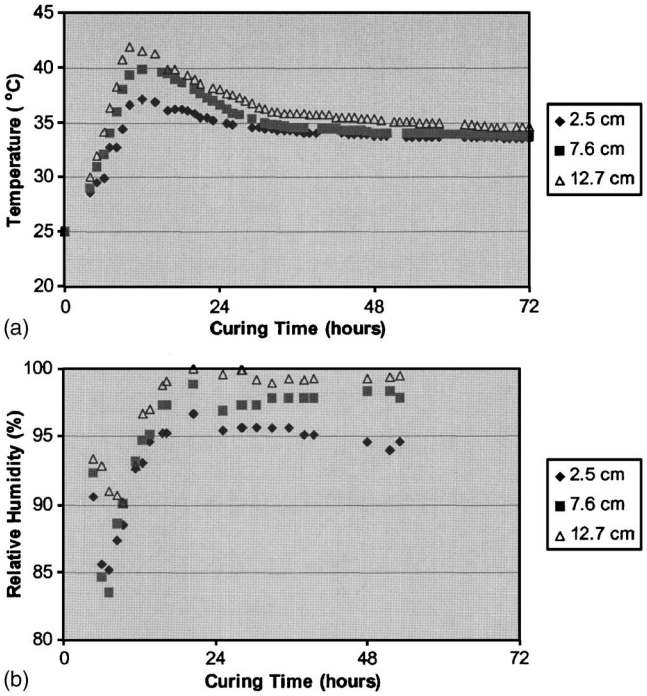


**Fig. 5.** Measured concrete temperature and relative humidity (laboratory): (a) temperature; (b) relative humidity



J. Mater. Civ. Eng. 2006.18:317-324.

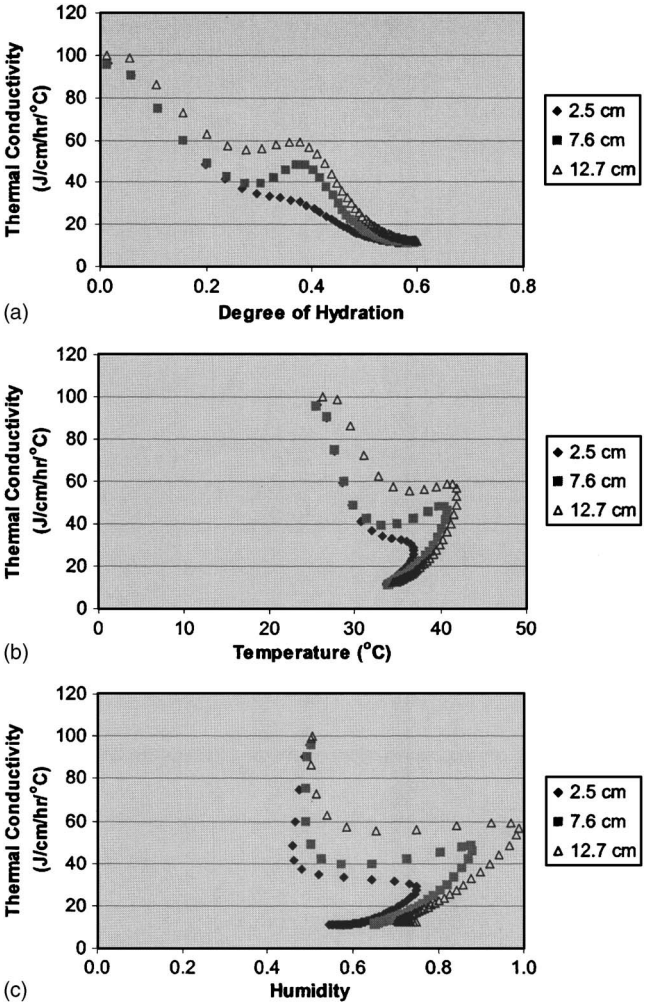


**Fig. 6.** Factors influencing thermal conductivity: (a) degree of hydration; (b) temperature; and (c) humidity

and moisture at 27.9 cm (11 in.) were assumed to be the same as those measured at 12.7 cm (5 in.) to form the polynomial fits, which allowed for interpolation or extrapolation of the temperature and moisture for other time steps and positions other than those where measurements were made. Using the concrete temperature profile functions, thermal conductivities were back-calculated by Eq. (21). As shown in Fig. 6, the deeper the measurement point from the slab top surface, the slightly higher is the thermal conductivity.

Thermal conductivity has been generally considered a function of moisture content in concrete or a linear function of the degree of hydration (Hsieh et al. 1989; Trinhztfy et al. 1982). The back-calculated thermal conductivity varied with temperature in addition to moisture and degree of hydration, as shown in Fig. 6. Therefore, the back-calculated thermal conductivity ($k$) was modeled as a function of temperature ($T$), humidity ($H$), and degree of hydration ($\alpha$) of concrete as

$$k = a \ln\left[\frac{1}{\alpha}\left(-\ln\frac{1}{T}\right)^{H}\right] + b \tag{22}$$

where $a$ and $b$=laboratory-derived coefficients. The thermal conductivity predicted by Eq. (22) corresponds to the back-calculated thermal conductivity [Eq. (21)] with high $R$-square values, as shown in Fig. 7.

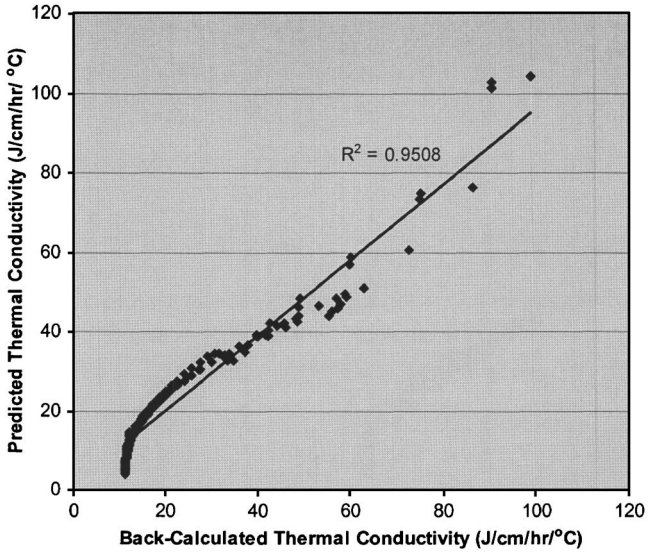


**Fig. 7.** Back-calculated versus predicted thermal conductivity

### *Model Validation*

The temperature of the test slab was forward-calculated using the thermal conductivity model, other material properties, and initial and boundary conditions. Input parameters to simulate the temperature of the test slab are summarized in Table 1. The typical ranges of value for each parameter are also shown in the table, with the exception of the parameters, which sensitively vary with mix proportions. The surface humidity predicted by Eq. (12) and humidity data stays between ambient and concrete humidity during the period of measurement, as shown in Fig. 8. The effective curing thickness of the test slab estimated by Eq. (11) and humidity data decreases with curing time as shown in Fig. 9.

To consider heat loss due to evaporation in the boundary condition at the slab top surface, the rate of evaporation of the test slab was calculated by Eqs. (6)–(12) and the data collected from the test slab (Jeong and Zollinger 2005). The variation of the evaporation rate shown in Fig. 10 indicates that a substantial amount of evaporation occurred in the afternoon of the day of the slab placement due to weather conditions and then decreased considerably the next day. The rate of evaporation also cycled between a maximum peak in the afternoon and minimum peak in the morning. Condensation and moisture absorption by the slab surface was made in the morning due to higher humidity and dew

**Table 1.** Summary of Input Parameters

| Parameters | Typical ranges (Neville 1996) | Value used |
|---|---|---|
| Initial temperature, $T_0$ (°C) | 2–32 | 29.8 |
| Density, $\rho$ (g/cm$^3$) | 2.2–2.6 | 2.286 |
| Specific heat, $c_p$ (J/g/°C) | 0.84–1.17 | 1.044 |
| Absorptitivity, $\alpha_s$ | 0.5–0.8 | 0.5 |
| Emissivity, $\epsilon$ | 0.80–0.95 | 0.9 |
| Total heat, $H_u$ (J/g) | 250–420 | 385 |
| Cement content, $C$ (g/cm$^3$) | 0.28–0.34 | 0.289 |
| Activation energy, $E$ (kJ/mol) | — | 31.4 |
| Parameter, $\lambda_1$ | — | 0.69 |
| Parameter, $\kappa_1$ | — | 1.52 |
| Parameter, $t_1$ | — | 13 |



J. Mater. Civ. Eng. 2006.18:317-324.

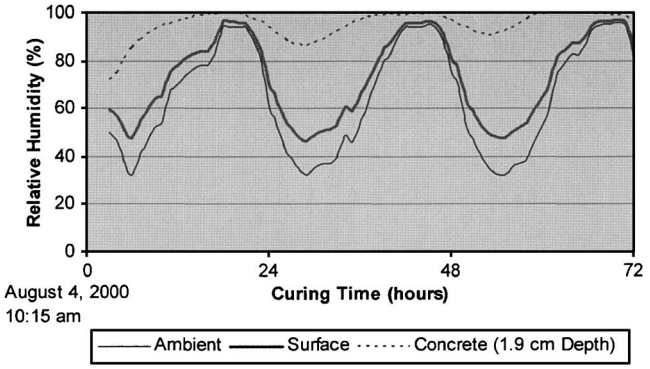


**Fig. 8.** Predicted surface relative humidity of test slab

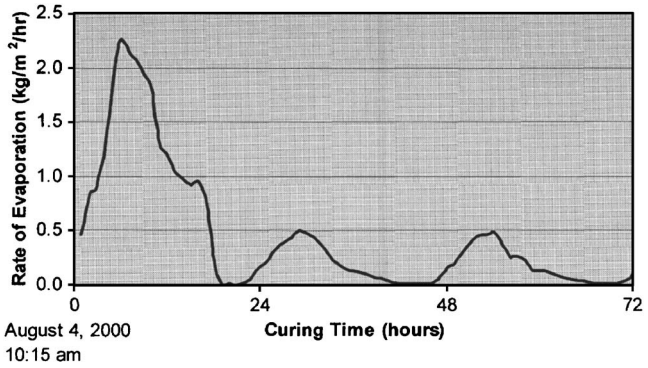


**Fig. 10.** Predicted rate of evaporation from test slab

point temperature of the ambient than those of the slab surface. The absorbed moisture evaporated in the afternoon, generating a higher rate of evaporation than in the morning. Fig. 11 shows the effects of the heat flux due to evaporation on the predicted results. It is clear that the temperature profiles predicted by TMAC[2] correspond to the temperature profiles measured in the field reasonably well, as shown in Fig. 12. The predicted profiles can be easily transmitted to analytical software for stress and deformation evaluation.

## Conclusions

The temperature distributions in early-age concrete pavement under specified environmental conditions are predicted by a 2D finite-element program, TMAC[2]. Heat flux due to evaporation was included in the boundary condition of heat transfer at the slab top surface by modeling surface humidity, effective curing thickness, surface moisture emissivity, and rate of evaporation. Thermal conductivity was back-calculated by transforming the governing equation of heat transfer and analyzing the data collected from laboratory testing. Theoretically, the back-calculated thermal conductivity represents the heat movements in concrete. Thus, the model of back-calculated thermal conductivity can be used in the calibration of predicted temperature of curing concrete pavements under various curing conditions and mixture proportions. Calculated temperature profiles corresponded to the temperature profiles measured at the test slab, but further improvements are warranted through better quality of field data and additional calibration efforts.

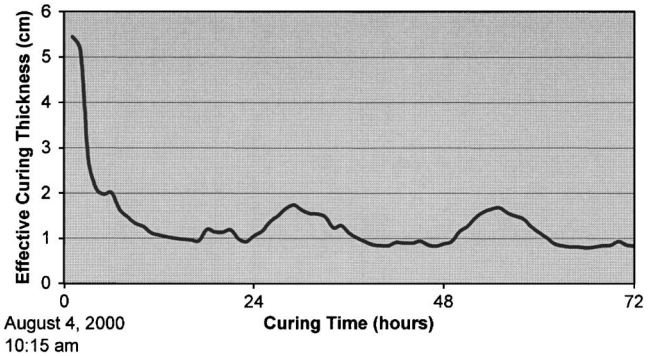


**Fig. 9.** Predicted effective curing thickness of test slab

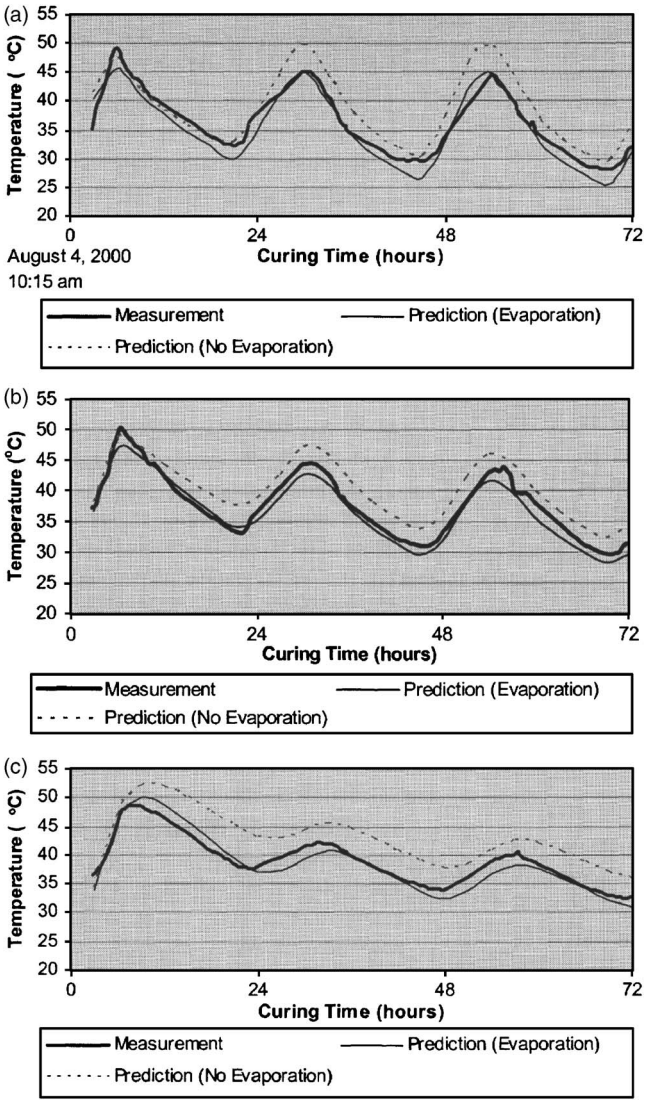


**Fig. 11.** Measured versus predicted temperature histories of test slab: (a) 2.5 cm (1 in.) from top; (b) 7.6 cm (3 in.) from top; and (c) 17.8 cm (7 in.) from top



J. Mater. Civ. Eng. 2006.18:317-324.

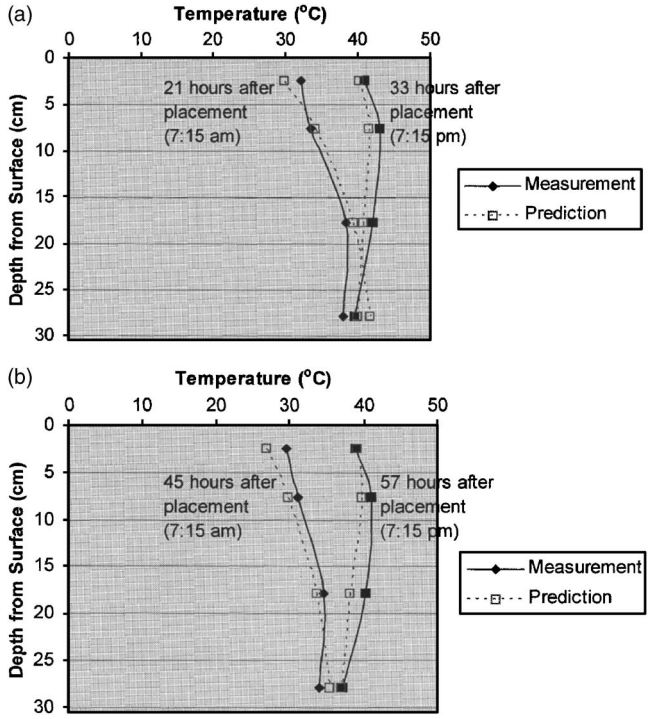


**Fig. 12.** Measured versus predicted temperature profiles of test slab: (a) 1 day after placement; (b) 2 days after placement

## Acknowledgments

The research in this paper was sponsored by the Federal Highway Administration (FHwA) and the Texas Department of Transportation (TxDOT). The writers express gratitude to the FHwA and TxDOT for their financial support.

## References

American Society of Heating Refrigeration and Air Conditioning Engineers (ASHRAE). (1972). *Handbook of fundamentals*, New York.

ASTM. (1999). "Standard practice for estimating concrete strength by the maturity method." *ASTM C1074, annual book of ASTM standards*, West Conshohocken, Pa.

Bathe, K. J. (1982). *Finite element procedures in engineering analysis*, Prentice-Hall, Englewood Cliffs, N.J.

Bazant, Z. P., and Najjar, L. J. (1972). "Nonlinear water diffusion in nonsaturated concrete." *Mater. Struct.*, 5(25), 3–20.

Branco, F. A., Mendes, R. A., and Mirabell, E. H. (1992). "Heat of hydration effects in concrete structures." *ACI Mater. J.*, 89(2), 139–145.

Chapman, A. J. (1982). *Fundamentals of heat transfer*, Macmillan, New York.

Emborg, M. (1989). "Thermal stresses in concrete structures at early ages." Doctoral's thesis, Lulea Univ. of Technology, Lulea, Sweden.

Hsieh, C. K., Qin, C., and Ryder, E. E. (1989). "Development of computer modeling for prediction of temperature distribution inside concrete pavements." *Rep. FL/DOT/SO/90-374*, Dept. of Mechanical Engineering, Univ. of Florida, Gainesville, Fla.

Incropera, F. P., and DeWitt, D. P. (1996). *Fundamentals of heat and mass transfer*, 4th Ed., Wiley, New York.

Jeong, J. H. (2003). "Characterization of slab behavior and related material properties due to temperature and moisture effects." Ph.D. dissertation, Texas A&M Univ., College Station, Tex.

Jeong, J. H., and Zollinger, D. G. (2003). "Development of test methodology and model for evaluation of curing effectiveness in concrete pavement construction." *Transportation Research Record. 1861*, Transportation Research Board, Washington D.C., 18–25.

Jeong, J. H., and Zollinger, D. G. (2005). "Environmental effects on the behavior of jointed plain concrete pavements." *J. Transp. Eng.*, 131(2), 140–148.

Kapila, D., Falkowsky, J., and Plawsky, J. L. (1997). "Thermal effects during the curing of concrete pavements." *ACI Mater. J.*, 94(2), 119–128.

Kaviany, M. (1994). *Principles of convective heat transfer*, Springer, New York.

Klemens, P. G. (1969). *Theory of the thermal conductivity of solids*, R. P. Tye, ed., Vol. 1, Academic, London.

Linsley, R. K., Kohler, M. A., and Paulhus, J. L. (1975). *Hydrology for engineers*, 2nd Ed., McGraw-Hill, New York.

Meinel, A. B., and Meinel, M. P. (1976). *Applied solar energy: An introduction*, Addison-Wesley, Reading, Mass.

Neville, A. M. (1996). *Properties of concrete*, 4th Ed., Wiley, New York.

Parrott, L. J. (1988). "Moisture profiles in drying concrete." *Adv. Cem. Res.*, 1(3), 164–170.

Parrott, L. J. (1991). "Factors influencing relative humidity in concrete." *Mag. Concrete Res.*, 43(154), 45–52.

Reddy, J. N. (1984). *Energy and variational methods in applied mechanics*, Wiley, New York.

Reddy, J. N. (1993). *An introduction to the finite element method*, 2nd Ed. McGraw-Hill, New York.

Ruiz, J. M., Schindler, A. K., Rasmussen, R. O., Nelson, P. K., and Chang, G. K. (2001). "Concrete temperature modeling and strength prediction using maturity concepts in the FHwA HIPERPAV software." *Proc., 7th Int. Conf. on Concrete Pavements*, 97–111.

Says, W. M., and Crawford, M. E. (1980). *Convective heat and mass transfer*, McGraw-Hill, New York.

Siegel, R., and Howell, J. R. (1981). *Thermal radiation heat transfer*, 2nd Ed., McGraw-Hill, New York.

Taljaston, B. (1987). "Temperature development and maturity growth for ordinary Swedish portland cement Type II." *Diploma Work 1987:035*, Technical Univ. of Lulea, Lulea, Sweden.

Timoshenko, S. P., and Goodier, J. N. (1970). *Theory of elasticity*, 3rd Ed., McGraw-Hill, New York.

Trinhztfy, H. W., Blaauwendraad, J., and Jongendijk, J. (1982). "Temperature development in concrete structures taking accounting of state dependent properties." *Proc., RILEM Int. Conf. on Concrete at Early Ages*, Vol, 1, RILEM, Cachon Cedex, France, 211–218.

Yang, S. (1996). "A temperature prediction model in new concrete pavement and new test method for concrete fracture parameters." Ph.D. dissertation, Texas A&M Univ., College Station, Texas.



J. Mater. Civ. Eng. 2006.18:317-324.